INTERNATIONAL JOURNAL OF PRECISION ENGINEERING AND MANUFACTURING Vol. 18, No. 10, pp. 1363-1370 OCTOBER 2017 / 1363
REGULAR PAPER
DOI: 10.1007/s12541-017-0162-9
ISSN 2234-7593 (Print) / 2005-4602 (Online)

A Parametric and Accurate CAD Model of Flat End Mills Based on Its Grinding Operations

Liming Wang[1,2,#], Lin Kong[1,2], Jianfeng Li[1,2], and Zezhong Chen[3]

1 Key Laboratory of High Efficiency and Clean Mechanical Manufacture of Ministry of Education, Jinan, 250061, China
2 School of Mechanical Engineering, Shandong University, Jinan, 250061, China
3 Department of Mechanical and Industrial Engineering, Concordia University, Montreal, Quebec, Canada
Corresponding Author / E-mail: liming_wang@sdu.edu.cn, TEL: +86-531-88392003, FAX: +86-531-88392003

KEYWORDS: End mill, Milling simulation, Grinding processes

End mills are widely used in CNC machining. However, the complex structures of end mills make it difficult to define the CAD model which determines the quality and performance of virtual cutting tests. This paper presents an accurate CAD model of end mill through analyzing kinematic models of grinding processes. Initially, a common parametric representation of grinding wheel is given. Base on the given wheel profile and the design parameters of cutters including the rake angle, core diameters and pitch angle, the representation of helix flute surface is first calculated using contact theory and also the formulation of rake angle and pitch angle are investigated. Next, four design parameters are used to control the shape of the gash which is formed via Boolean operation between the given wheel and end mill. Similarly, the peripheral edges and end edges are swept using grinding simulation. Finally, integrating all the above processes, a parametric CAD model of end mill is represented. The simulation results showed that the proposed CAD model could achieve 1e-3 mm and 2e-2 deg. in accuracy, which can be used to evaluate the grinding process or improve the future FEA analysis of end-mills.

Manuscript received: November 3, 2016 / Revised: March 25, 2017 / Accepted: May 27, 2017

NOMENCLATURE

R = grinding wheel radius
[dx dy dz] = grinding wheel position
β = grinding wheel orientation
r_T = cutter radius
r_c = cutter core radius
γ = flute rake angle
γ_e = end rake angle
ϕ = flute angle
η = gash angle
α_p = peripheral relief angle
α_e = end relief angle

1. Introduction

Milling is used widely in a variety of industrial applications to machine complex surface and remove large amounts of material.[1,2] The performance of milling process is determined by the mechanism which can be modeled through the intersection between the machining tool structures and the work-piece.[3-6] However, because of the complex structures of end mill, most of researches for the milling process are based on the simplified CAD models which use the lines and arcs to approximate the basic cutting angles.[7,8] The geometrical model of end mill is the basis of further engineering analysis, such as finite element analysis of cutting performances. Besides, some researchers also pointed out that accurate models of cutting tools used in the machining processes are required to precisely simulate the machining operations.[9] Therefore, developing the accurate geometrical model of end mill is very important.

End mill is generally manufactured using the CNC grinding machine. With the advance of CNC technology, the precision of cutter is increasing, and it also brings kinds of geometrical features, such as the gashes, variable pitches.[10-12] There are some papers focusing on the grinding methods of end mill, mainly building the flute shape. Kaldor[13] first discussed two basic problems in the flute-grinding processes: determination of the resulting flute profile for a given grinding wheel

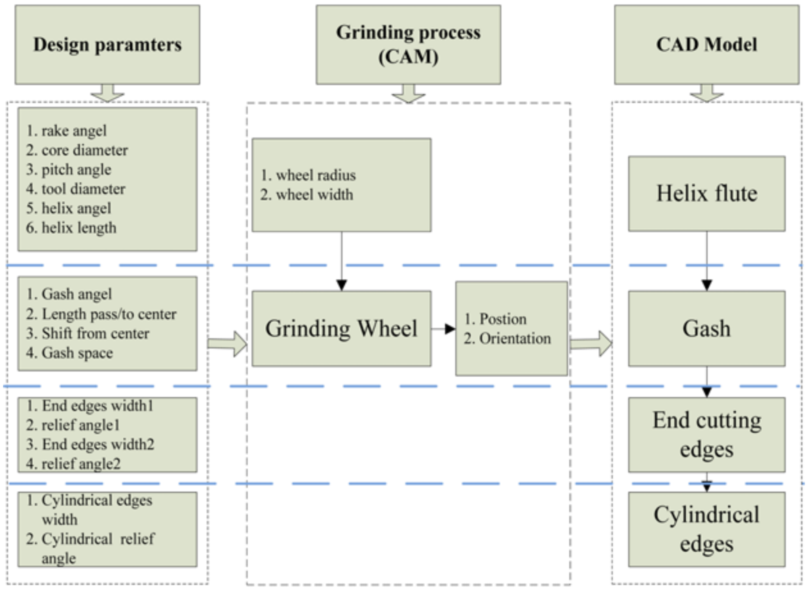

Fig. 1 Scheme of modelling end mills

and determination of the wheel profile for a desired flute cross-section. Chen[14] presented a method to grind rake face of taper end mill using spherical grinding wheel. Nevertheless, most of those researches focus on shaping the helix flutes without considering the gashes and edge features. It is difficult to model the exact three dimensional shape of an end mill because a certain part of the shape is not determined until the actual machining stage.[15,16] In this work, the paper was organized as following. First, a parametric CAD model is provided base on the grinding processes including the helix flute, gashes and cutting edges through modeling the kinematic of the grinding operations. Second, the CAD model was verified by the CNC grinding experiments. Finally, to address the accuracy and benefits of proposed CAD model, the cutting forces prediction in milling simulation was carried out with different methods.

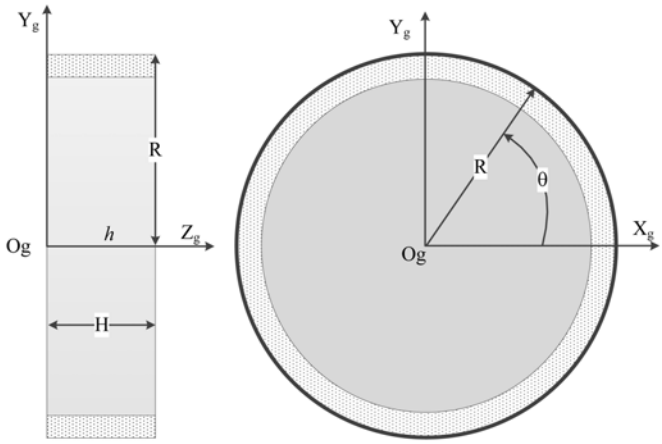

Fig. 2 Profile of standard grinding wheel

2. Framework of Modeling End-Mills

Five or four axis CNC grinding machine is employed to construct the grinding processes of end mils and the NC programming is generated automatically through the specific commercial CAM software in industry. Basically, four main plans are required to finish grinding of end mill, that is, flute-grinding, gash-grinding, end cutting-edges-grinding and cylindrical cutting edges-grinding.[10] In this paper, the framework of modeling the end-mills were shown in Fig. 1. The first layer is the design parameters, including the basic information of the end-mills, such as, tool diameters rake angles, relief angle, and so no, of which values should be provided by the designers. The second layer is the grinding operations which is aimed to program the planning of grinding processes to satisfy the requirement of the design parameters provided by the first layer. In the second layer, the main task is to determine the proper geometry of grinding wheel and develop the kinematics of grinding processes. The third layer is the CAD system, which is used to generate the solid model of end-mill through calculation of the swept volume of the grinding wheel at different position and orientation provided by the second layer. Finally, the CAD model for solid end-mills was accomplished layer by layer.

The shape of end mill is formed through grinding between cutting tool and grinding wheel. Thus proper wheel geometries must be determined prior to machining the helical flute for the end mills designed. In mass production, the grinding wheels are standardized into several types. A wheel coordinate system $\boldsymbol{O_g}$-$\boldsymbol{X_g Y_g Z_g}$ is established to represent the grinding wheel in a parametric form in Fig. 2. Then, the grinding wheel can be represented in the wheel coordinate system in Eq. (1). The wheel surface normal $\boldsymbol{N_g}$ can be obtained in Eq. (2).

$$W_g(h,\theta) = \begin{bmatrix} R\cdot\cos\theta \\ R\cdot\sin\theta \\ h \end{bmatrix} \tag{1}$$

where R is the wheel radius, h and are the wheel parametric variables with $h \in [0, \mathrm{H}]$, $\theta \in [0, 2\pi]$.

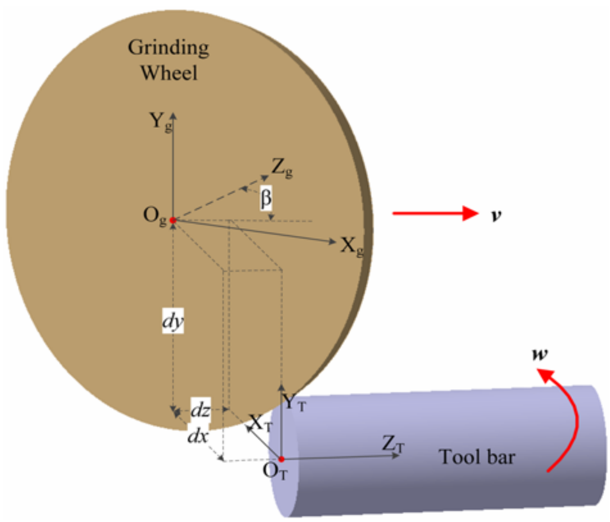

Fig. 3 Illustration of the flute-grinding operations

$$N_g = \begin{bmatrix} \cos\theta \\ \sin\theta \\ 0 \end{bmatrix} \tag{2}$$

3. Grinding Processes and Mathematical Modeling

3.1 Flute modeling

The helix flute grinding is the most important step in the entire end mill manufacturing process, since it forms important parameters such as rake angel, core diameter, pitch angle, and helix angle.[11] In practice, the flute is machined by the grinding wheel moving with a helix motion. In this work, the grinding processes are modeling, and all the parameters are calculated using the contact theory.

To demonstrate the configuration and machining processes, two coordinate systems are set up, one is moving coordinate system $\mathbf{O_g}$, which has been mentioned in the above wheel coordinate system. And another is tool coordinate system denoted by $\mathbf{O_T}$. As shown in Fig. 3, the grinding wheel is set by rotating about the $\mathbf{Y_T}$ axis by the wheel set-up angel β and translating by a vector [dx dy dz]. Therefore, the initial setting of the grinding wheel can be expressed by homogenous coordinate transformation matrix in Eq. (3). After configuration, the work-piece rotates about tool axis $\mathbf{Z_T}$ in a specific angular velocity ω, while grinding wheel translates along $\mathbf{Z_T}$ axis in a specific translation velocity v. The corresponding equivalent matrix is expressed in Eq. (4).

$$\mathbf{M}_1 = trans(\mathrm{Z_T}, dz)\cdot trans(\mathrm{Y_T}, dy)\cdot trans(\mathrm{X_T}, dx)\cdot rot(\mathrm{Y_T}, \beta) = \begin{bmatrix} \cos\beta & 0 & \sin\beta & dx \\ 0 & 1 & 0 & dy \\ -\sin\beta & 0 & \cos\beta & dz \\ 0 & 0 & 0 & 1 \end{bmatrix} \tag{3}$$

$$\mathbf{M}_2(t) = \begin{bmatrix} \cos(\omega\cdot t) & -\sin(\omega\cdot t) & 0 & 0 \\ \sin(\omega\cdot t) & \cos(\omega\cdot t) & 0 & 0 \\ 0 & 0 & 1 & v\cdot t \\ 0 & 0 & 0 & 1 \end{bmatrix} \tag{4}$$

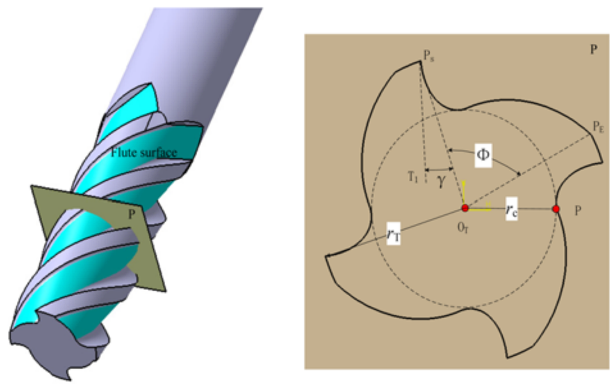

Fig. 4 Definition of flute parameters in the flute cross-section

where, t is the machining time.

As aforementioned, the flute surface is generated by intersection between the tool and the grinding wheel in a helix motion. In this operation, at any instant, the grinding wheel is contacting the flute surface with a curve which is called contact curve in this work. The contact curve can be derived in the tool coordinate system based on kinematic relation of the grinding wheel and the work-piece using contact theory in Eq. (5).

$$\boldsymbol{N_T}\cdot\boldsymbol{V_T} = 0 \tag{5}$$

Where, $\boldsymbol{N_T}$ is the normal of the grinding wheel surface in the tool coordinate system and can be obtained through transform of $\boldsymbol{N_g}$.

The flute surface can be obtained through integrating all the above equations and expressed in Eq. (6).

$$S_{flute} = \begin{bmatrix} dx\cdot\cos(\omega t) - dy\cdot\sin(\omega t) + h\cdot\sin\beta\cdot\cos(\omega t) \\ -R\cdot\sin\theta^*\cdot\sin(\omega t) + R\cdot\cos\beta\cdot\cos\theta^*\cdot\cos(\omega t) \\ dx\cdot\sin(\omega t) + dy\cdot\cos(\omega t) + h\cdot\sin\beta\cdot\sin(\omega t) \\ +R\cdot\sin\theta^*\cdot\cos(\omega t) + R\cdot\cos\beta\cdot\cos\theta^*\cdot\sin(\omega t) \\ h\cdot\cos\beta + vt - R\cdot\sin\beta\cdot\cos\theta^* \end{bmatrix} \tag{6}$$

Generally, the flute parameters including rake angle, core radius and flute angle are defined within the cross-section. As shown in Fig. 4, the flute profile is described in the reference of the tool coordinate system. In order to define the flute parameters, two key points is illustrated as following: The start point P_S and end point P_E of the flute are the intersection of flute profile with the tool boundary. The flute angle f refers to the open angle $\angle P_S O_T P_E$ between the start point P_S and end point P_E, which can be expressed using the vector form in Eq. (7).

$$\phi = a\cos\left(\frac{O_T P_S\cdot O_T P_E}{|O_T P_S|\cdot|O_T P_E|}\right) \tag{7}$$

The core radius is the minimum distance from the flute curve to origin O_T, which can be calculated using the following expression in Eq. (8).

$$r_c = min(sqrt(x^2+y^2))\text{, where } [x,y]\in S_{flute} \tag{8}$$

Besides, the rake angle g is also calculated as the angle between the tangent TP_S shown in Eq. (9) and radius direction $P_E O_T$ at point P_S.

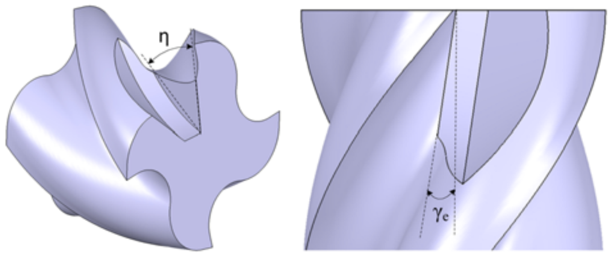

Fig. 5 Illustration of gash angle and end rake angle

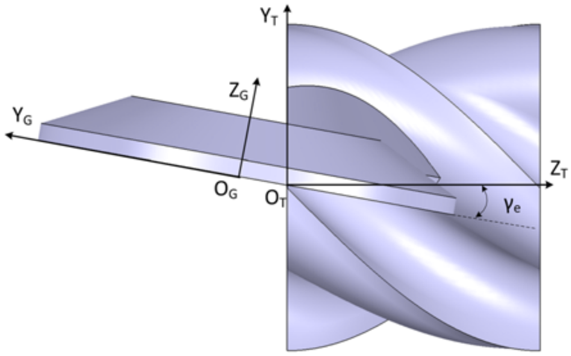

Fig. 6 Configuration of the gash-grinding operations

$$\gamma = \cos^{-1}\left(\frac{TP_S \cdot P_E O_T}{|TP_S| \cdot |P_E O_T|}\right) \tag{9}$$

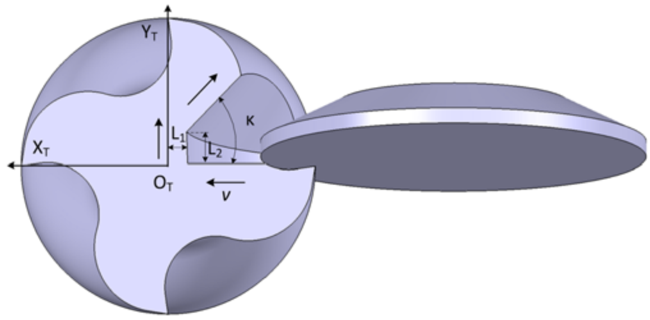

Fig. 7 Illustration of the gash-grinding operations

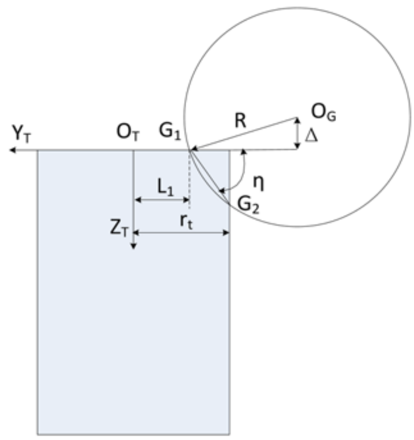

Fig. 8 Scheme of grinding the gash angle

3.2 Gash modeling

From the literature review, there are few papers discussing the gash model. Gash is locating at the bottom of end mill and it provides the chip space while feeding axially in milling processes. Besides, the distribution of gashes determines the type of end tooth, such as long tooth and short tooth. The geometry of the gash is governed by two critical parameters: end rake angle denoted by η and axial gash angle γ_e in Fig. 5.

Comparing to the flute-grinding processes, gash is formed simply at the bottom of end mill. As shown in Fig. 6, initially, the wheel coordinate system is in coincidence with the tool coordinate system. Then, the grinding wheel is configured by rotating about the $\mathbf{X_T}$ axis by a set-up angle 90-γ_e, and finally it translates by a distance Δ in the direction of O_GO_T. Similar to the flute-grinding, an equivalent matrix $\mathbf{M_4}$ is introduced to represent this operation:

$$\mathbf{M}_4 = \begin{bmatrix} 1 & 0 & 0 & 0 \\ 0 & \sin\gamma_e & -\cos\gamma_e & \Delta\cdot\sin\gamma_e \\ 0 & \cos\gamma_e & \sin\gamma_e & -\Delta\cdot\cos\gamma_e \\ 0 & 0 & 0 & 1 \end{bmatrix} \tag{10}$$

After configuration, as shown in Fig. 7, the grinding wheel translates by a distance L_1 in the $\mathbf{X_T}$ direction, and then goes to the $\mathbf{Y_T}$ direction by a distance L_2, finally, exits according to the exit angle κ. In this process, the gash angle η is determined. Noting that, in Fig. 7, the distance L_1 is off to the tool center, which means the corresponding teeth is short. If L_1 is passing the tool center, it will be a long tooth.

In this work, Boolean operation between the grinding wheel and the tool is employed to develop the gash CAD model. In the gash modeling, only two Boolean operations is enough to simulate this process accurately. One operation is used at the translating distance L_1, and another is at the translating distance L_2.

The gash angle is formed when the grinding wheel reach the distance L_1 in Fig. 8. And, the gash angle is ground by the larger end of the grinding wheel. From a geometric view, the kinematic relation between the grinding wheel and the tool can be illustrated with a geometric model shown in |Fig. 8. The circle in the figure represents the larger end of grinding wheel, and it is intersected with the tool at two points G_1 and G_2. The gash angle is regards as the angle between vectors G_1G_2 with the negative Y_T axis.

The larger end of grinding wheel is expressed by Eq. (11) in the tool coordinate system.

$$\mathbf{E}_\mathrm{T}(\theta) = \begin{bmatrix} R\cdot\cos\theta - L_1 - \sqrt{R^2-\Delta^2} \\ R\cdot\sin\theta - \Delta \end{bmatrix} \tag{11}$$

The point G_1 is calculated through Eq. (11) by setting $R\cdot\sin\theta - \Delta = 0$:

$$\mathbf{G_1} = \begin{bmatrix} -L_1 \\ 0 \end{bmatrix} \tag{12}$$

Similarly, Let $R\cdot\cos\theta - L_1 - \sqrt{R^2-\Delta^2} = -r_t$ in Eq. (11), we get:

$$\theta^*_{G_2} = a\cos\left[\frac{L_1 + \sqrt{R^2-\Delta^2} - r_t}{\mathrm{R}}\right] \tag{13}$$

Fig. 9 three types of cutting edges: concave, flat and eccentric

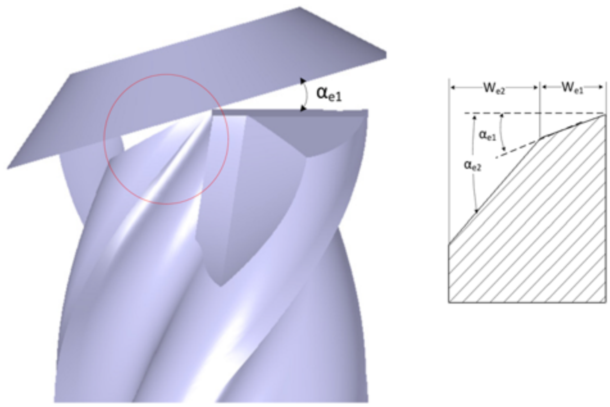

Fig. 10 Illustration of grinding end cutting edges

Substituting $\theta^*_{G_2}$ into Eq. (11), point G_2 is obtained expressed by Eq. (14).

$$\mathbf{G}_2 = \begin{bmatrix} R\cdot\cos(\theta^*_{G_2}) - L_1 - \sqrt{R^2-\Delta^2} \\ R\cdot\sin(\theta^*_{G_2}) - \Delta \end{bmatrix} \quad (14)$$

Since point G_1 and G_2 is found, it is easily to represent the vector G_1G_2 in Eq. (15).

$$\mathbf{G}_1\mathbf{G}_2 = \begin{bmatrix} R\cdot\cos(\theta^*_{G_2}) - \sqrt{R^2-\Delta^2} \\ R\cdot\sin(\theta^*_{G_2}) - \Delta \end{bmatrix} \quad (15)$$

The formula of gash angle is shown in Eq. (16)

$$\eta = a\tan\left[\frac{\frac{\Delta}{R} - \sin(\theta^*_{G_2})}{\cos(\theta^*_{G_2}) - \sqrt{1-\left(\frac{\Delta}{R}\right)^2}}\right] \quad (16)$$

3.3 Cutting edge modeling

In metal cutting processes, cutting edges are the most important factors which greatly affect cutting efficiency. Comparing to the flute geometric shape, the cutting edges are easier to be grounded. And, the relief angle defined on the corresponding flank surfaces are formed in this grinding process. Generally, according to different grinding methods, the cutting edges can be classified into three types: concave, flat and eccentric shown in Fig. 9. In this study, the flat cutting edges are discussed. For the cylindrical end mill, the cutting edges are composed of two parts: the end cutting edges and the peripheral cutting edges.

Basically, for each tooth, there are two cutting edges, generally called the first cutting edge and the second cutting edge which are defined by the corresponding relief angle (α_{e1}, α_{e2}) and cutting width (We_1, We_2). As shown in Fig. 10, the first end cutting edges are ground by the larger end of grinding wheel. The wheel is set up by an angle α and then

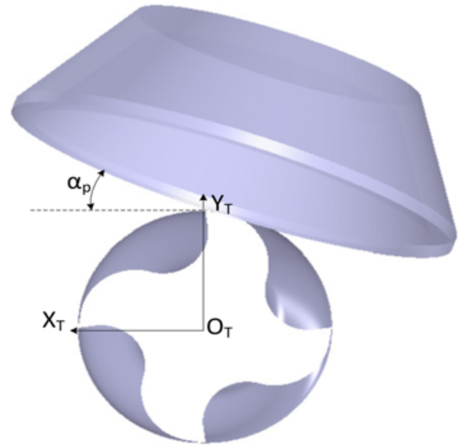

Fig. 11 Illustration of grinding peripheral cutting edges

translates along the cutting edges. Obviously, the set-up angle α_{e1} is determined by the first end relief angle. The second cutting edge is grounded with the same operation. And the geometric relation between the two cutting edges is demonstrated using a break view shown in Fig. 10.

Similarly, the peripheral cutting edges are ground via helix motion which is result from the translation of the grinding wheel and the rotation of the tool shown in Fig. 11. And, the helix motion is governed by Eq. (4). In this process, the peripheral relief angle α_p and width w_p is obtained. The mathematical expression of the flank surface is derived in Eq. (17).

$$\mathbf{F}(\mu,t) = \begin{bmatrix} w_p\cdot\mu\cdot\cos(t) - \left(r_T - w\cdot\tan(\alpha_p)\cdot\mu\right)\cdot\sin(t) \\ w_p\cdot\mu\cdot\sin(t) + \left(r_T - w\cdot\tan(\alpha_p)\cdot\mu\right)\cdot\cos(t) \\ r_T\cdot\cot\lambda\cdot t \end{bmatrix} \quad (17)$$

Where, $\mu \in [0, 1]$, α_p is the relief angle and w_p is the relief surface width.

4. Verification

In the above sections, a solid CAD integrated model of end-mill was proposed based on modeling its grinding operations. In order to verify the proposed model, both the CAM simulation and grinding experiments were conducted to design a four-flute end-mill in this work. The setting parameters for CNC grinding including the grinding wheel dimension and its location, as well as setting-up angle β are illustrated in Table 1. The CAM simulation was implemented with the volume-sweep function in 3D software CATIA with the proposed mathematical models. As shown in Fig. 12(a), the solid CAD models was obtained including flutes, cutting edges, gash and tool bar were rendered with different colors. The corresponding parameters of the solid model are also measured in CATIA shown Fig. 12(b). Besides, the designed end-mill was manufactured with Walter CNC grinding machine with the proposed grinding parameters shown in Fig. 12(c). The tool parameters for the manufactured cutter were measured with the equipment JTVMS2010 shown in Fig. 12(d) and the measure results

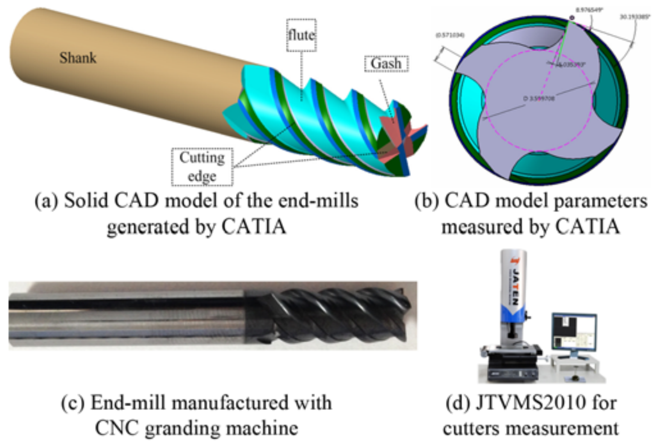

Fig. 12 Verification of the proposed CAD model

Table 1 Setting parameters for CNC grinding operations (length unit: mm, angle unit: deg.)

CNC Operations	Wheel parameters	Wheel position [dx dy dz]	Set up angle β
Flute-grinding	R=75 H=20	[28.963 64.716 -31.258]	49.20
Flank-grinding	R=50 H=15	[9.218 58.199 0.000]	0.00
Gash-grinding	R=75 H=20	[-37.400 1.899 -54.094]	10.00

Table 2 Comparisons of the developed CAD model and manufactured cutter (length unit: mm, angle unit: deg.)

Tool parameters	Designed cutter	Developed CAD model	Manufactured cutter
Total length	60.000	60.000	60.030
Flute length	18.000	18.000	18.120
Tool diameter	6.000	6.000	6.010
Helix angle	45.00	45.00	45.12
Rake angle	5.00	5.02	5.38
Core diameter	3.600	3.600	3.610
1st Relief angle	9.00	8.98	9.82
2nd Relief angle	30.00	30.19	30.68
1st Land width	0.550	0.571	0.595
End rake angle	10.00	10.00	10.02
Gash angle	42.00	42.02	42.12

were tabulated in Table 2. To address the accuracy of the proposed model, the comparison between the proposed CAD model and real cutter was listed in Table 2, which showed that the difference between the designed cutter and the built CAD model could achieve 1e-3mm and 2e-2 deg. in accuracy, which satisfy the tolerances requirement of end-mill design and manufacture.

5. Application

To investigate the accuracy of the proposed model, the cutting forces in the milling simulation were predicted with the proposed CAD model and the simplified CAD model in the FEA shown in Fig. 13. The FEA software used in this research is ThirdWave AdvantEdge, which is a powerful commercial CAE software devoted on metal cutting simulation.

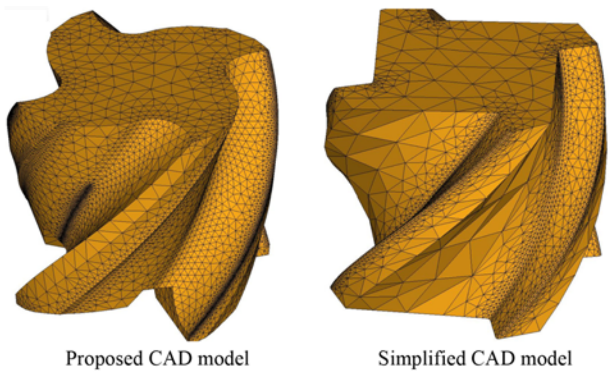

Fig. 13 The proposed CAD model and simplified CAD model for end-mills

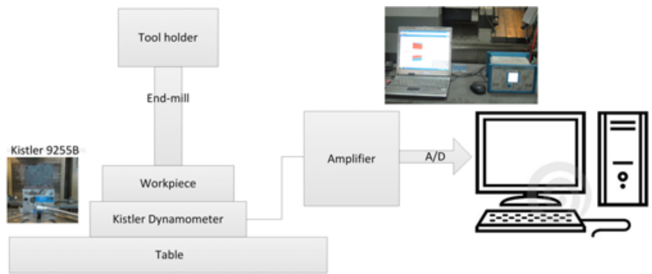

Fig. 14 Cutting forces measurement with the manufactured cutter

Table 3 Material properties of the end-mill and work-piece

Material properties	End-mill	Work-piece
Material	Tungsten carbide	AISI4140 Alloy steel
Modulus of elasticity	690 GPa	200 GPa
Poisson's ratio	0.24	0.3
Density	14800 kg/m^3	7850 kg/m^3
Hardness, Brinell	2570 N/mm^2	1049 N/mm^2
Yield strength	-	821 MPa
Ultimate tensile strength	-	1073 MPa

In this application, AISI4140, a typical high strength material applied widely in aeronautic industry, was used as an experimental material to predict the cutting forces in the milling simulation. The properties of the materials and cutting tools are pre-defined shown in Table 3. The milling processing parameters was set as cutting depth 3 mm, cutting width 1.2 mm, feed rate 0.06 mm/tooth and spindle speed 8000 rpm. In order to save simulation time, the 3D cutter models are truncated with the effective cutting lengths (5 mm) and imported to the software with stp format. Besides, as shown in Fig. 14, the cutting forces were also obtained from experiments use the manufactured cutter of Fig. 12(c) to compare with the FEA simulation results.

The cutting forces predicted with different methods were plotted in Fig. 15, respectively. It showed that the cutting forces predicted by the proposed CAD model were in better agreement with the experiments than the simplified CAD model. The average deviation of cutting forces between the proposed CAD model simulation and the experiments was around 10%, which can be acceptable as an estimation to evaluate the cutting performance for the end-mill design.

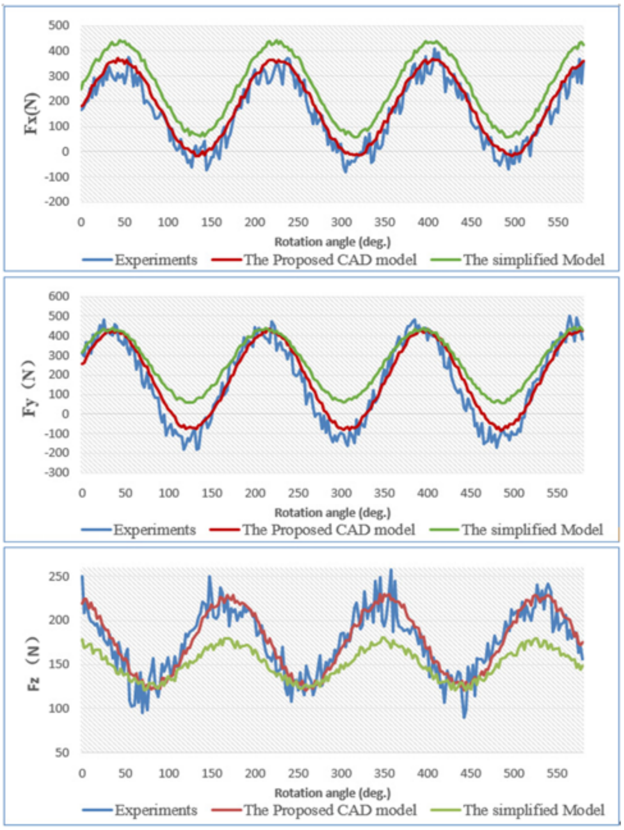

Fig. 15 Cutting forces prediction with different methods

6. Conclusions

In this paper, a parametric CAD model of flat end mill is proposed based on its grinding processes. The exact flute shape model is represented via the explicit equation using contact theory between the given grinding wheel and the tool. And the representation of the rake angle and pitch angle in the cross-section of helix flute are derived. Besides, a more detail mathematical model of the gash including the machine configuration and grinding processes is first proposed in this study. The actuate CAD model can be utilized as a fundamental part of virtual simulation to improve the quality of tool, such as the prediction of cutting force and the suppression of chatter in machining processes using FEA method. And another application is to be integrated with CAM system to generate NC code for grinding end mill in a CNC machine.

ACKNOWLEDGEMENT

This work was partially supported by the China Postdoctoral Science Foundation (NO.2016M592182), the Fundamental Research Funds of Shandong University (NO. 2015HW020) and Shandong Provincial Natural Science Foundation, China (NO.ZR2017BEE018).

REFERENCES

1. Yıldız, A. R., "An Effective Hybrid Immune-Hill Climbing Optimization Approach for Solving Design and Manufacturing Optimization Problems in Industry," Journal of Materials Processing Technology, Vol. 209, No. 6, pp. 2773-2780, 2009.
2. Kobayashi, Y. and Shirai, K., "Multi-Axis Milling for Micro-Texturing," Int. J. Precis. Eng. Manuf., Vol. 9, No. 1, pp. 34-38, 2008.
3. Dotcheva, M., Dotchev, K., and Popov, I., "Modelling and Optimization of Up-and Down-Milling Processes for a Representative Pocket Feature," Int. J. Precis. Eng. Manuf., Vol. 14, No. 5, pp. 703-708, 2013.
4. Yildiz, A. R., "A New Hybrid Differential Evolution Algorithm for the Selection of Optimal Machining Parameters in Milling Operations," Applied Soft Computing, Vol. 13, No. 3, pp. 1561-1566, 2013.
5. Yildiz, A. R., "Cuckoo Search Algorithm for the Selection of Optimal Machining Parameters in Milling Operations," The International Journal of Advanced Manufacturing Technology, Vol. 64, Nos. 1-4, pp. 1-7, 2013.
6. Yildiz, A. R., "A New Hybrid Artificial Bee Colony Algorithm for Robust Optimal Design and Manufacturing," Applied Soft Computing, Vol. 13, No. 5, pp. 2906-2912, 2013.
7. Chen, W.-Y., Chang, P.-C., Liaw, S.-D., and Chen, W.-F., "A Study of Design and Manufacturing Models for Circular-Arc Ball-End Milling Cutters," Journal of Materials Processing Technology, Vol. 161, No. 3, pp. 467-477, 2005.
8. Li, G., Sun, J., and Li, J., "Process Modeling of End Mill Groove Machining Based on Boolean Method," The International Journal of Advanced Manufacturing Technology, Vol. 75, Nos. 5-8, pp. 959-966, 2014.
9. Li, A., Zhao, J., Pei, Z., and Zhu, N., "Simulation-Based Solid Carbide End Mill Design and Geometry Optimization," International Journal of Advanced Manufacturing Technology, Vol. 71, Nos. 9-12, pp. 1889-1900, 2014.
10. Tandon, P. and Khan, M. R., "Three Dimensional Modeling and Finite Element Simulation of a Generic End Mill," Computer-Aided Design, Vol. 41, No. 2, pp. 106-114, 2009.
11. Wang, L. and Chen, Z., "A New CAD/CAM/CAE Integration Approach to Predicting Tool Deflection of End Mills," International Journal of Advanced Manufacturing Technology, Vol. 72, Nos. 9-12, pp. 1677-1686, 2014.
12. Wang, L., Chen, Z. C., Li, J., and Sun, J., "A Novel Approach to Determination of Wheel Position and Orientation for Five-Axis CNC Flute Grinding of End Mills," The International Journal of Advanced Manufacturing Technology, Vol. 84, Nos. 9-12, pp. 2499-2514, 2016.
13. Kaldor, S., Rafael, A. M., and Messinger, D., "On the CAD of Profiles for Cutters and Helical Flutes-Geometrical Aspects," CIRP Annals-Manufacturing Technology, Vol. 37, No. 1, pp. 53-56, 1988.

14. Chen, F. and Bin, H., “A Novel CNC Grinding Method for the Rake Face of a taper Ball-End Mill with a CBN Spherical Grinding Wheel,” The International Journal of Advanced Manufacturing Technology, Vol. 41, Nos. 9-10, pp. 846-857, 2009.

15. Kim, J. H., Park, J. W., and Ko, T. J., “End Mill Design and Machining Via Cutting Simulation,” Computer-Aided Design, Vol. 40, No. 3, pp. 324-333, 2008.

16. Li, G., Sun, J., and Li, J., “Modeling and Analysis of Helical Groove Grinding in End Mill Machining,” Journal of Materials Processing Technology, Vol. 214, No. 12, pp. 3067-3076, 2014.